Supplementary Information for

Amorphization and Defect Engineering of Nb_2O_5 within a Graphitic Nanocage Array for Catalytic Polysulfide Conversion in Lithium–Sulfur Batteries

*Yifan Gao,[†a] Hao Wang,[†b] Dong Yang,[a] Wenqian Han,[*b] Tongtao Li,[*b] and Angang Dong[*b]*

[a]State Key Laboratory of Molecule Engineering of Polymers and Department of Macromolecular Science, Fudan University, Shanghai 200438, China.

[b]State Key Laboratory of Porous Materials for Separation and Conversion and Department of Chemistry, Shanghai Key Laboratory of Molecular Catalysis and Innovative Materials and iChEM, Fudan University, Shanghai 200438, China.

[†]These authors have contributed equally to this work.

*Corresponding author: wqhan@fudan.edu.cn; ttli@fudan.edu.cn; agdong@fudan.edu.cn

Experimental Section

Materials

All chemicals were used as received without further purification. Sublimed sulfur, N-methyl-2-pyrrolidone (NMP), and Li_2S were purchased from Sigma-Aldrich. Sodium oleate was purchased from TCI. NaCl (99.99%) and ammonium niobate oxalate hydrate ($C_4H_4NNbO_9 \cdot xH_2O$, 99.99%) were purchased from Aladdin. N-lauryl acrylate (LA133) binder, and polyvinylidene fluoride (PVDF) binder were purchased from Chengdu Yindile Power Supply Technology. Carbon paper was purchased from Suzhou Sinero Technology CO., LTD. Super P, Celgard 2400 (PP) separators, and electrolytes were purchased from DoDochem. The electrolyte was composed of 1.0 M lithium bis (trifluoromethanesulfonyl) imide (LiTFSI) in 1, 3-dioxolane (DOL) and dimethoxymethane (DME) (1:1 by volume) with 2 wt% $LiNO_3$ additive.

Synthesis of Nb_2O_5@MGF membranes

The MGF was synthesized through a template-directed transformation of 2D Fe_3O_4 NCSLs, following a modified literature protocol.[1] The Nb_2O_5@MGF composite was synthesized through a spatially confined growth method within the cubic carbon cages of the MGF framework. In a typical process, 20 mg of MGFs was mixed with 40 mg of ammonium niobate oxalate hydrate in 10 mL of oxalic acid aqueous solution (pH=4) under sonication for 30 min. This treatment ensures the complete infiltration of the niobium precursor into the open mesoporous channels of the MGFs. Afterward, the mixture was dried at 75 °C overnight. The obtained solid was subsequently calcined at 450 °C for 2 hours under a N_2 atmosphere. This thermal treatment triggers the in-situ decomposition of the precursor, leading to the confined formation of Nb_2O_5 nanoparticles inside the individual carbon cages, which effectively prevents their aggregation.

Materials characterization

Transmission electron microscopy (TEM), high-resolution TEM (HRTEM), scanning TEM (STEM), and elemental mapping were carried out on a Tecnai G2 20 TWIN microscope operated at 200 kV. Scanning electron microscopy (SEM) was conducted

on a Zeiss Ultra-55 microscope operated at 5 kV. Powder X-ray diffraction (XRD) measurements were carried out on a Bruker D2 Phaser X-ray diffractometer. X-ray photoelectron spectroscopy (XPS) was conducted using a Perkin Elmer PHI-5000C ESCA system. N_2 adsorption-desorption isotherms were collected on a Tristar II 3020 instrument and the pore size distribution was derived using the Barrett-Joyner-Halenda (BJH) model. Raman spectra were recorded with an XploRA Raman system at room temperature. Thermogravimetric analysis (TGA) was conducted on a Perkin-Elmer Pyris 1 thermogravimetric analyzer with a heating rate of 10 ^{o}C min^{-1} under airflow. EPR experiments were performed on a Bruker A300-10/12 system. Sectioning of separators was carried out using FIB (LEICA EM TIC 3X). At room temperature, the contact angle measurements with liquid electrolytes were done on a DSA-25 drop shape analyzer (Kruss, USA).

Li-S battery assembly and electrochemical performance measurements

Preparation of S cathodes. Active sulfur impregnation was prepared by mixing CNT powder with sublimed sulfur in a 3:7 weight ratio. The resulting mixture was then sealed in a Teflon pot and subjected to heat treatment at 155 ^{o}C for 12 hours. The cathode slurries were prepared by mixing S/CNT, Super P, and PVDF (8:1:1 by weight) in NMP under vigorous stirring. The as-prepared slurry was cast onto Al foil and then dried at 60 ^{o}C under vacuum overnight. All of the cathodes had a sulfur loading of 1.5 mg cm^{-2} unless otherwise noted. The cathodes with high sulfur loadings can be prepared following the same procedures. The electrolyte/sulfur ratio was 6 μL mg^{-1} for electrodes with sulfur loading of 5 mg cm^{-2}.

PP separator modification. In a typical procedure, 4 mg of Nb_2O_5@MGF powder was dispersed in 10 mL of water/ethanol (1:1 by volume) under sonication for 30 min. Then, 25 mg of 2 wt% LA133 aqueous solution was added into the Nb_2O_5@MGF dispersion with continuous sonication. The resulting mixture was filtered onto the PP separator and dried at 60 ^{o}C for 12 h. Other coating materials, such as Nb_2O_5 and MGF, were used to modify PP separators, following the same procedure.

Electrochemical characterization. The experiments were conducted using coin-type half cells (2016R) that were assembled inside an Ar-filled glovebox. Li-foil served as the counter electrode. The electrolyte was the mixture of DOL and DME in a 1:1 volume ratio, with 1M LiTFSI and 2 wt% $LiNO_3$ as the dissolved additives.

Galvanostatic measurements were performed on a Neware cell test instrument, which cycled between 1.7 and 2.7 V at various current densities. Specific capacity values were calculated by the mass of sulfur. Cyclic voltammetry (CV) measurements were conducted using an Autolab N 204 electrochemical workstation. The measurements were taken at a scan rate of 0.1-0.5 mV s^{-1} in the voltage range of 1.7-2.7 V. All Li-S batteries underwent a single activation cycle at 0.05 C (1 C = 1675 mA g^{-1}) prior to electrochemical tests.

To determine the Li-ion diffusion rate, galvanostatic charge/discharge, and cyclic voltammetry measurements were conducted. The oxidation and reduction peak currents were found to have a linear correlation with the square root of the scan rate, which was analyzed using the Randles-Sevcik equation:

$$I_p = (2.69 \times 10^5) n^{1.5} A D_{Li^+}{}^{0.5} C_{Li} v^{0.5}$$

where I_p stands for the peak current, n is the charge transfer number, A refers to the active area of the electrode, D_{Li^+} represents the Li-ion diffusion coefficient, C_{Li} is the Li-ion concentration, and v refers to the scanning rate.

Symmetric-cell assembly and evaluation of the redox kinetics of polysulfides

The electrode slurries were prepared by mixing 1.5 mg of Nb_2O_5@MGF, 0.375 mg of KB with 9 μL of Nafion and 375 μL of ethanol, followed by sonication for 30 min. The slurries were applied onto 14 mm diameter, 300 μm thick carbon paper and vacuum-dried at 60 ºC for 12 h to form symmetric electrodes. The carbon paper coated with Nb_2O_5 and MGF was prepared following the same procedure. The 0.5 M Li_2S_6 electrolyte was prepared by mixing the S and Li_2S powder with the molar ratio of 5:1 in the mixing solvent of DOL and DME (1:1 by volume) at 60 ºC for 12 h under vacuum. The experiment utilized identical working and counter electrodes, with a mass loading of 1.2 mg cm^{-2}. The electrolyte consisted of 30 μL of 0.5 M Li_2S_6. The CV measurements for symmetric cells were measured between -1.0 V and 1.0 V at the scan rate of 5 mV s^{-1}.

Measurements of the Li_2S nucleation

Precipitation of Li_2S on Nb_2O_5, MGF, and Nb_2O_5@MGF was investigated in 2016R-coin cells, using 20 μL of 0.2 M Li_2S_8 electrolyte and Celgard 2400 PP membrane as separator. The cells were discharged at a constant current of 0.1 mA until reaching 2.06 V, followed by a potentiostatic discharge at 2.05 V until the current fell below 10^{-5}. The Li_2S nucleation capacity was calculated by integrating the area under the curve using Faraday's Law.

Measurements of the Li_2S dissolution

The cells after the Li_2S deposition test were disassembled and the cathodes were used to assemble new cells for the Li_2S dissolution test. The cells were assembled with identical electrolytes, separators and anodes. Firstly, the cells were galvanostatically discharged to 1.70 V at 0.10 mA, then galvanostatically discharged to 1.80 V at 0.01 mA to ensure the sufficient transformation of LiPSs into solid Li_2S on the catalyst surface. Afterwards, the cells were potentiostatically charged at 2.35 V until the charge current was below 10^{-5} A for the complete dissolution of Li_2S.

Density functional theory (DFT) calculations

We have employed the first-principles[2,3] to perform density functional theory (DFT) calculations within the generalized gradient approximation (GGA) using the Perdew-Burke-Ernzerhof (PBE)[4] formulation. We have chosen the projected augmented wave (PAW) potentials[5,6] to describe the ionic cores and take valence electrons into account using a plane wave basis set with a kinetic energy cutoff of 400eV. Partial occupancies of the Kohn−Sham orbitals were allowed using the Gaussian smearing method and a width of 0.05 eV. The electronic energy was considered self-consistent when the energy change was smaller than 10^{-4} eV. A geometry optimization was considered convergent when the energy change was smaller than 0.05 eV $Å^{-1}$. The vacuum spacing in a direction perpendicular to the plane of the structure is 18 Å for the Nb_2O_5 surface. The Brillouin zone integration is performed using 2×2×1 Monkhorst-Pack k-point sampling for a structure. Finally, the adsorption energies (E_{ads}) were calculated as $E_{ads} = E_{ad/sub} - E_{ad} - E_{sub}$, where $E_{ad/sub}$, E_{ad}, and E_{sub} are the total energies of the optimized

adsorbate/substrate system, the adsorbate in the structure, and the clean substrate, respectively. The free energy was calculated using the equation:

$$G = E_{ads} + E_{ZPE} - TS$$

where G, E, Z_{PE} and T_S are the free energy, total energy from DFT calculations, zero point energy and entropic contributions, respectively. Ab initio molecular dynamics (AIMD) simulation was carried out to study the Nb_2O_5 structure, respectively. During geometry optimization, the cut-off energy was set as 500 eV for structures, respectively. The Brillouin zone was sampled by a Monkhorst-Pack (MP) k-point grid of 1×1×1 for geometry optimizations. The PBE-D3 dispersion term was introduced to correct the van der Waals interactions. The conjugated gradient method was applied with a smearing width of 0.15 eV, and the convergence criteria for the energy and force were 10^{-4} eV/cell and 0.05 eV/Å, respectively. AIMD simulations were run for 20 ps as equilibration with time steps of 1 fs, performing a constant temperature of 300 K in the Nosé -Hoover isokinetic ensemble.

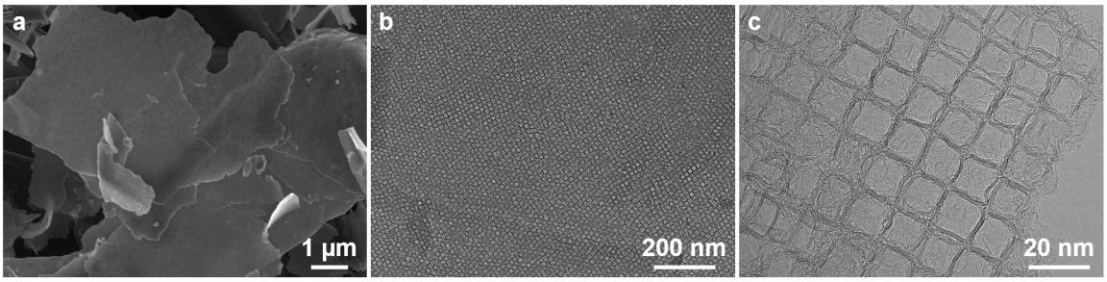

Figure S1. (a) SEM image, (b) TEM image, and (c) HRTEM image of MGF.

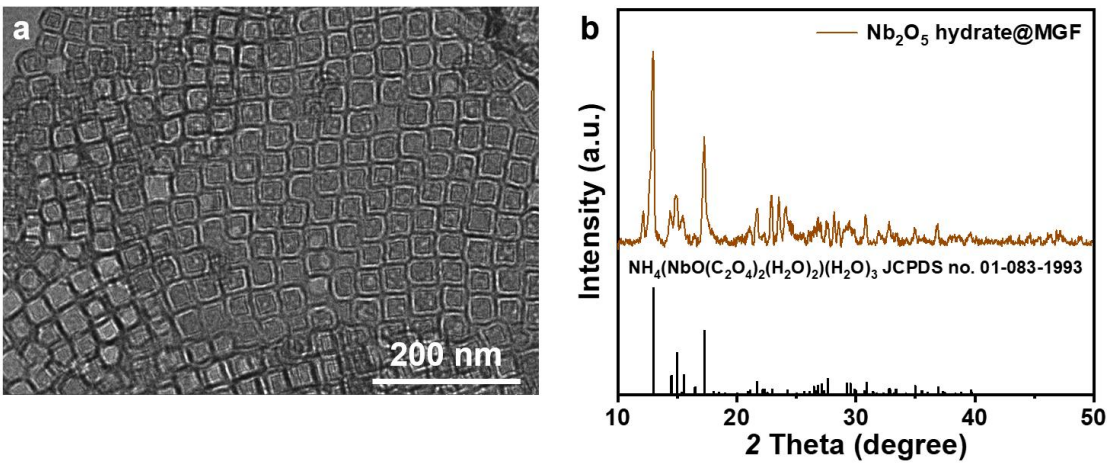

Figure S2. (a) TEM image and (b) XRD pattern of Nb_2O_5 hydrate@MGF.

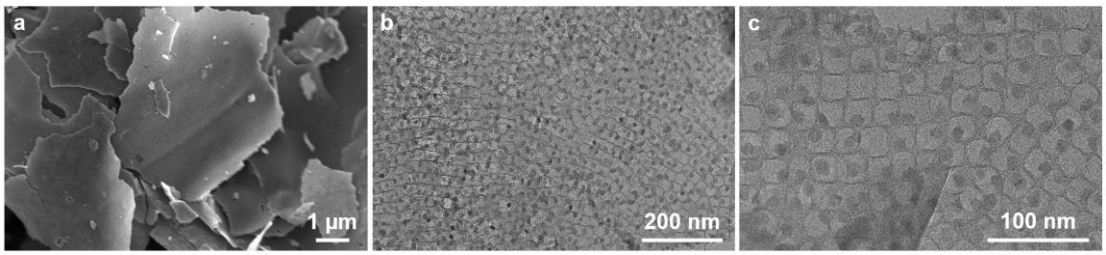

Figure S3. (a) SEM image, (b) TEM image, and (c) HRTEM image of Nb_2O_5@MGF.

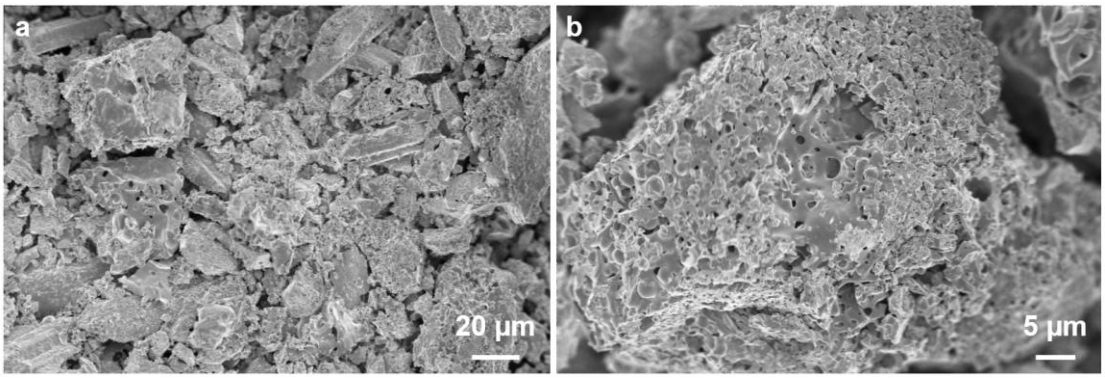

Figure S4. (a) Low- and (b) high-magnification SEM images of Nb_2O_5.

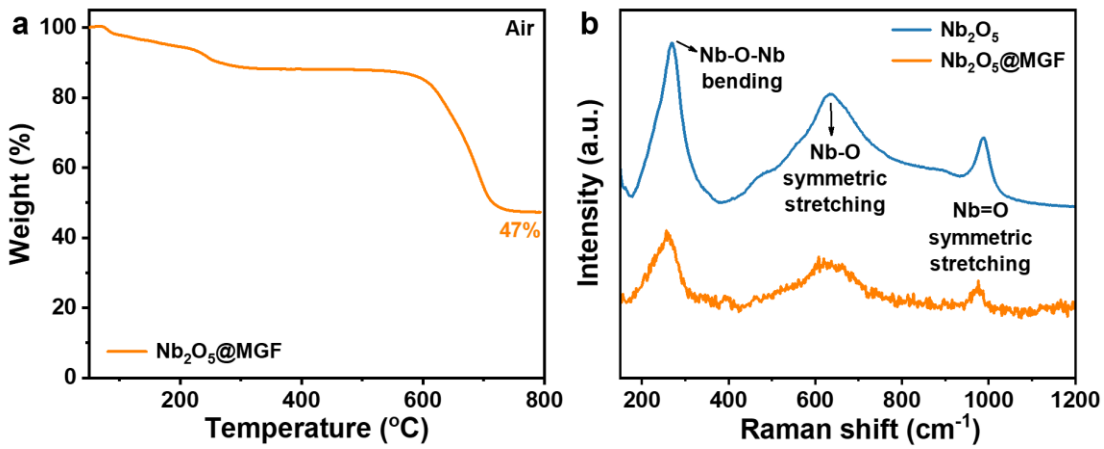

Figure S5. (a) TGA curve of Nb_2O_5@MGF. (b) Raman spectra of MGF and Nb_2O_5@MGF.

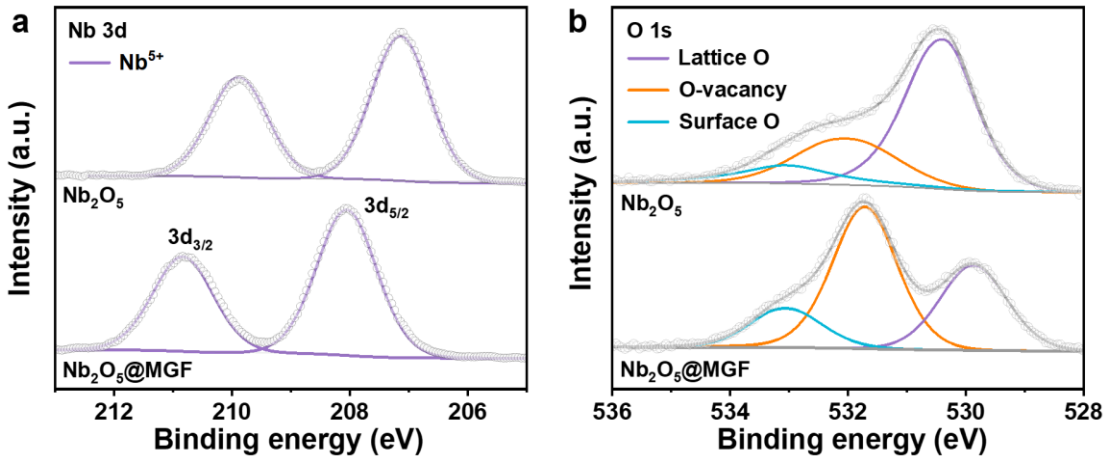

Figure S6. XPS spectra for (a) the Nb 3d region and (b) the O 1s region of Nb_2O_5 and Nb_2O_5@MGF.

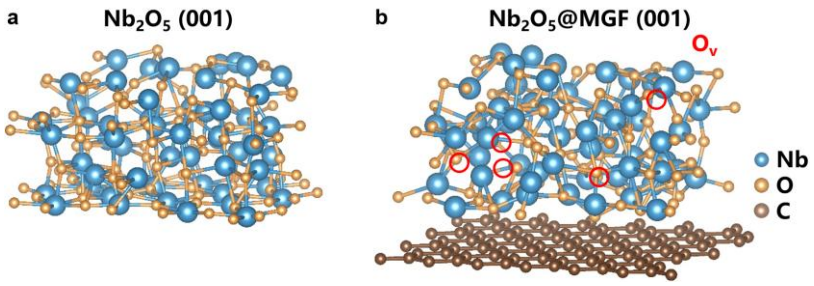

Figure S7. DFT calculation derived optimized adsorption configurations of (a) Nb_2O_5 (001) facet and (b) Nb_2O_5@MGF (001) facet.

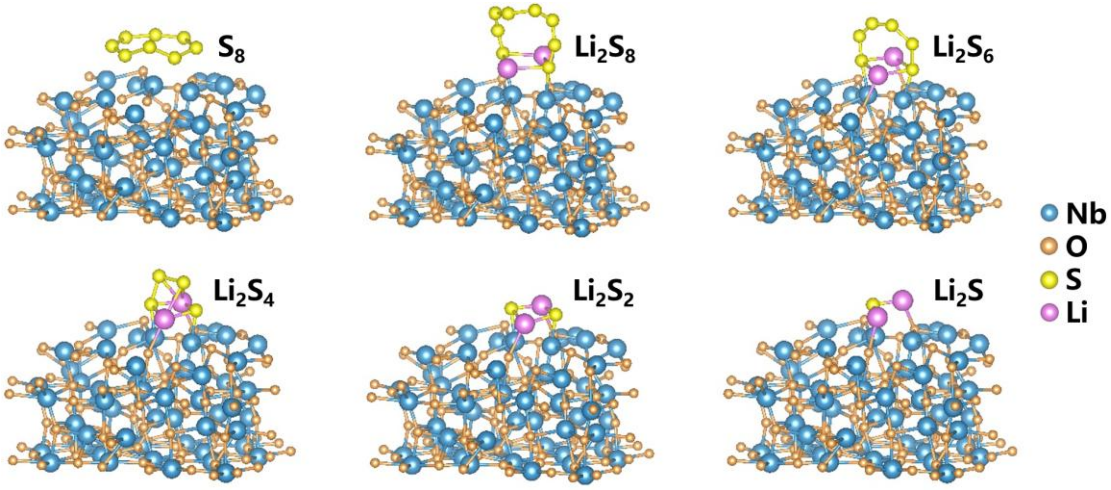

Figure S8. The optimized adsorption configurations of polysulfides on Nb_2O_5 (001) facet.

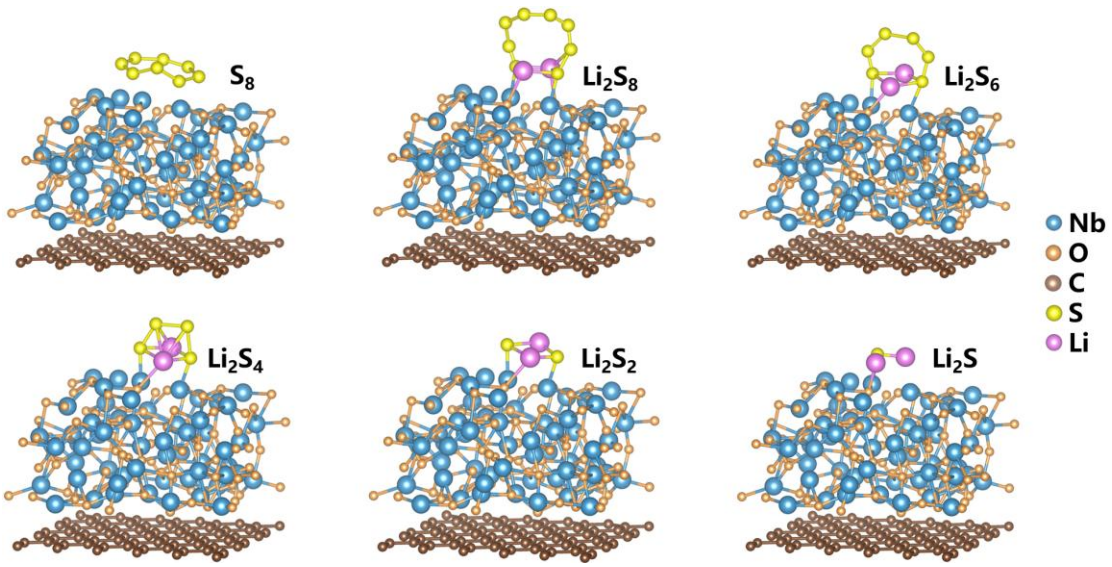

Figure S9. The optimized adsorption configurations of polysulfides on Nb_2O_5@MGF (001) facet.

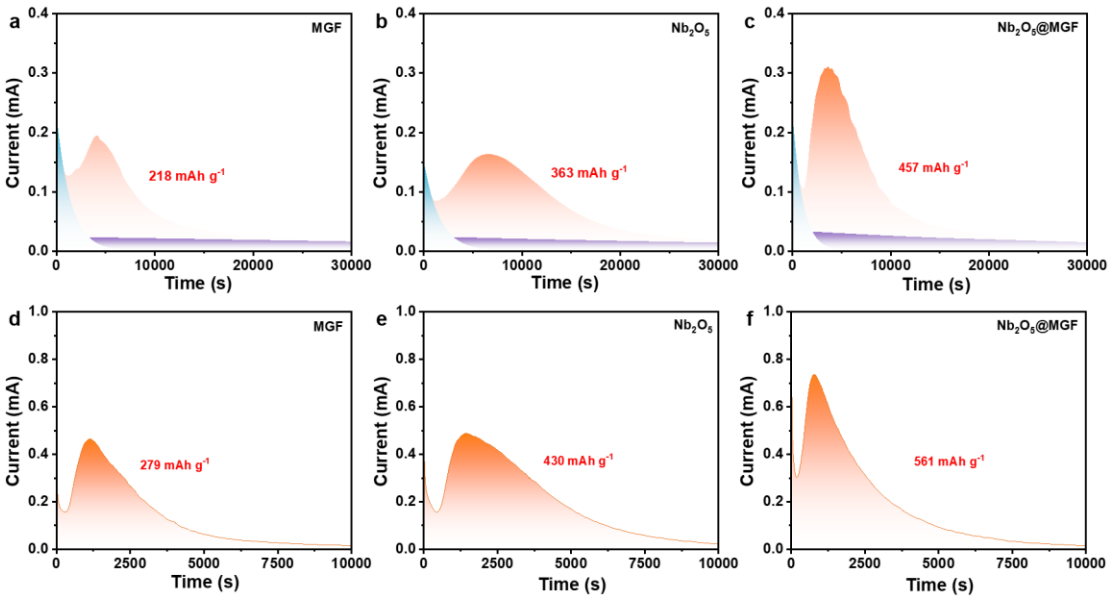

Figure S10. Potentiostatic discharge profiles of Li_2S nucleation of (a) MGF, (b) Nb_2O_5, and (c) Nb_2O_5@MGF. Potentiostatic discharge profiles of Li_2S dissolution of (d) MGF, (e) Nb_2O_5, and (f) Nb_2O_5@MGF.

The results show that Nb_2O_5@MGF exhibits the highest capacity for Li_2S nucleation and dissolution. This is attributed to its specific structure of amorphous, oxygen-deficient Nb_2O_5 confined in graphitic cages, which effectively facilitates the solid-to-liquid conversion.

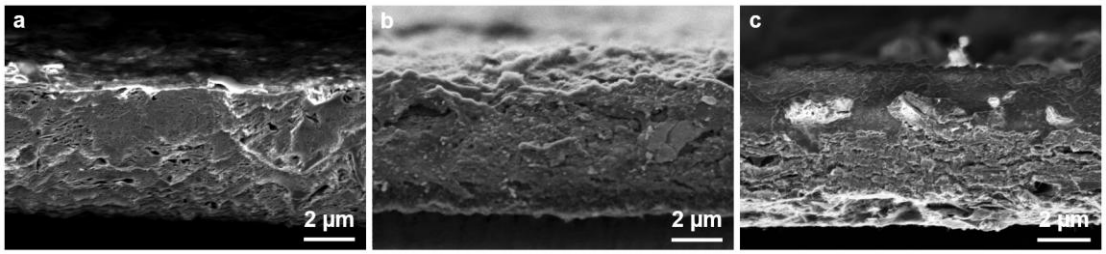

Figure S11. Cross-sectional SEM images of the interlayers with (a) MGF, (b) Nb_2O_5, and (c) Nb_2O_5@MGF.

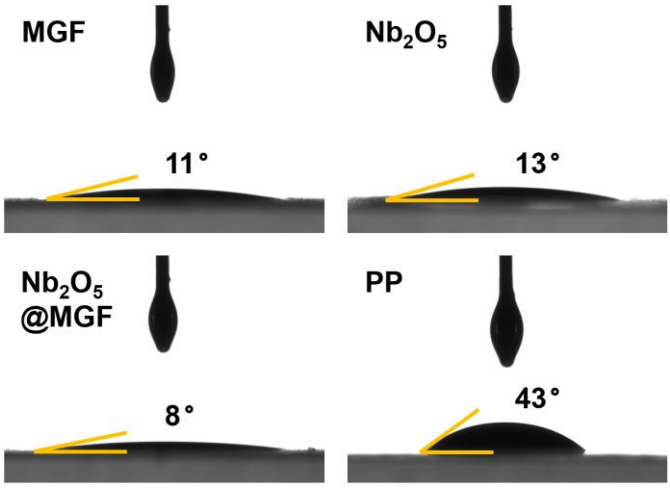

Figure S12. Contact angle measurements of various separators.

The Nb_2O_5@MGF interlayer demonstrates the most favorable wettability among the series, which is advantageous for Li^+ diffusion across the separator.

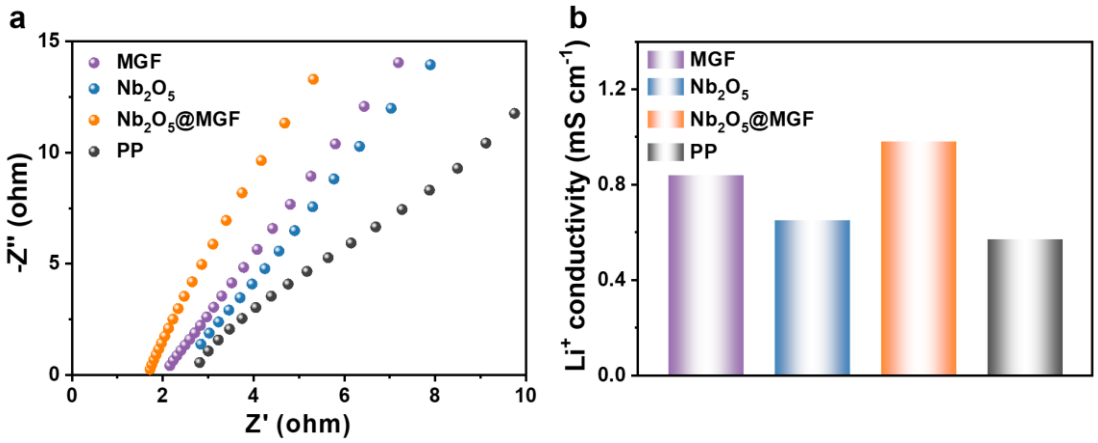

Figure S13. (a) Nyquist plots of stainless steel/separator/stainless steel cells assembled with various separators and (b) comparison of the ionic conductivities.

To determine the ionic conductivity measured by EIS with separators sandwiched between two stainless steel plates. The ionic conductivity was calculated according to the equation:

$$\sigma = d/(S \times R)$$

where d is the thickness of the separator, R is the bulk resistance, and S represents the contact area.

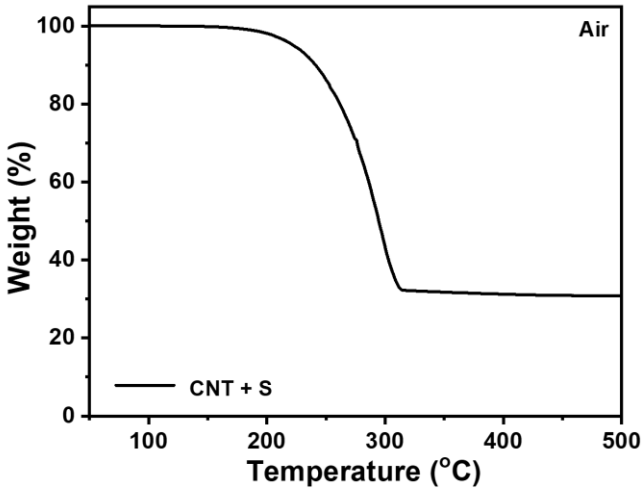

Figure S14. TGA curve of CNT/S cathodes, showing the sulfur content is ~70 wt%.

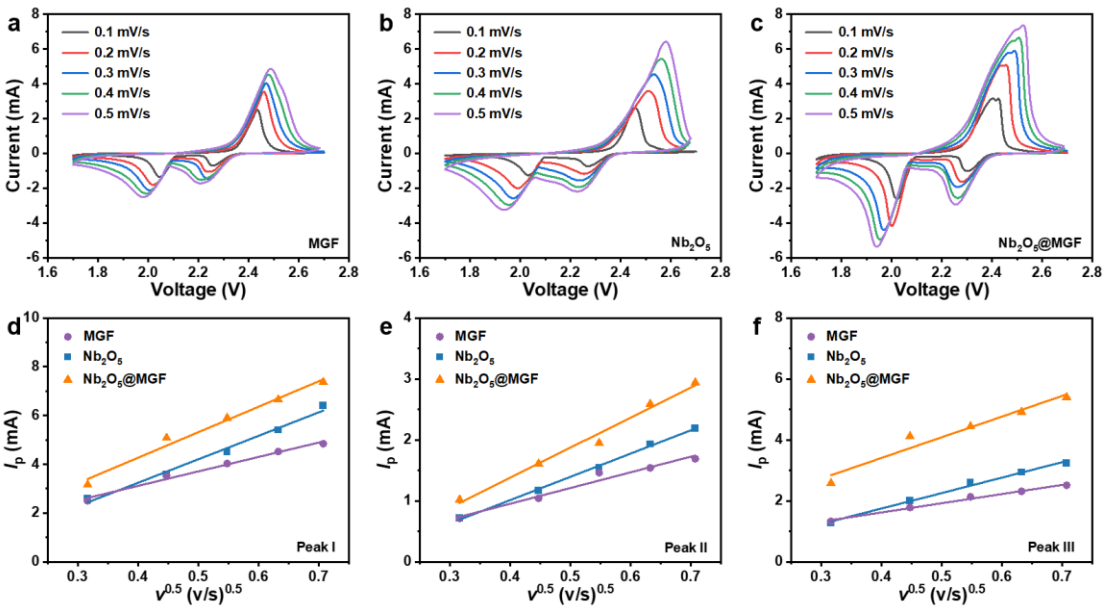

Figure S15. CV curves of LSBs with (a) MGF/PP, (b) Nb_2O_5/PP, and (c) Nb_2O_5@MGF/PP. Peak currents (I_p) vs. the square root of the scan rate ($v^{0.5}$): (d) Peak I, (e) Peak II, and (f) Peak III.

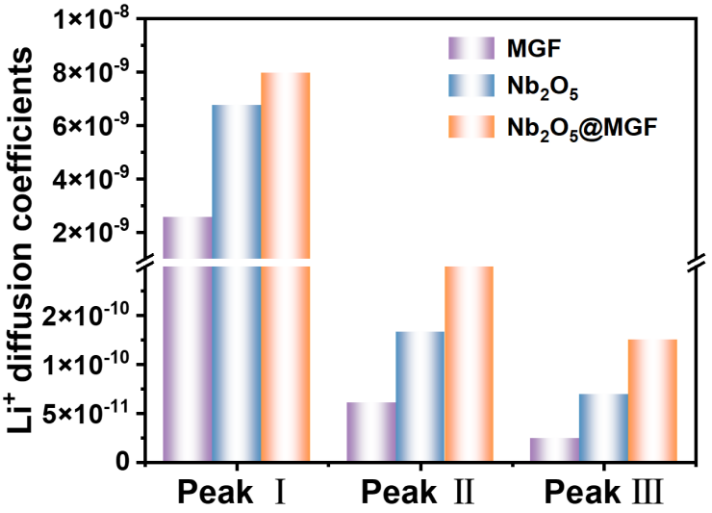

Figure S16. Li^+ diffusion coefficients derived from the three peaks of the CV curves.

It can be observed that the Nb_2O_5@MGF/PP battery exhibits the highest Li^+ diffusion coefficients for all three redox peaks, indicating that the Nb_2O_5@MGF interlayer significantly enhances the high-flux diffusion of Li^+, in line with its superior ionic conductivity.

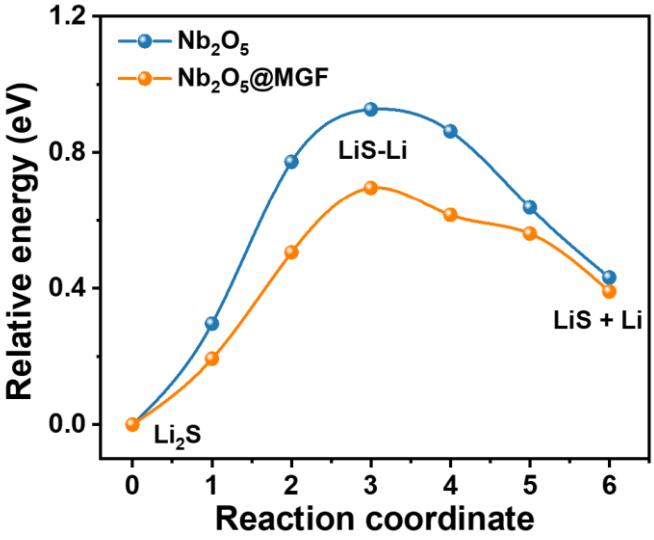

Figure S17. Energy profiles of the decomposition of Li_2S on Nb_2O_5 and Nb_2O_5@MGF.

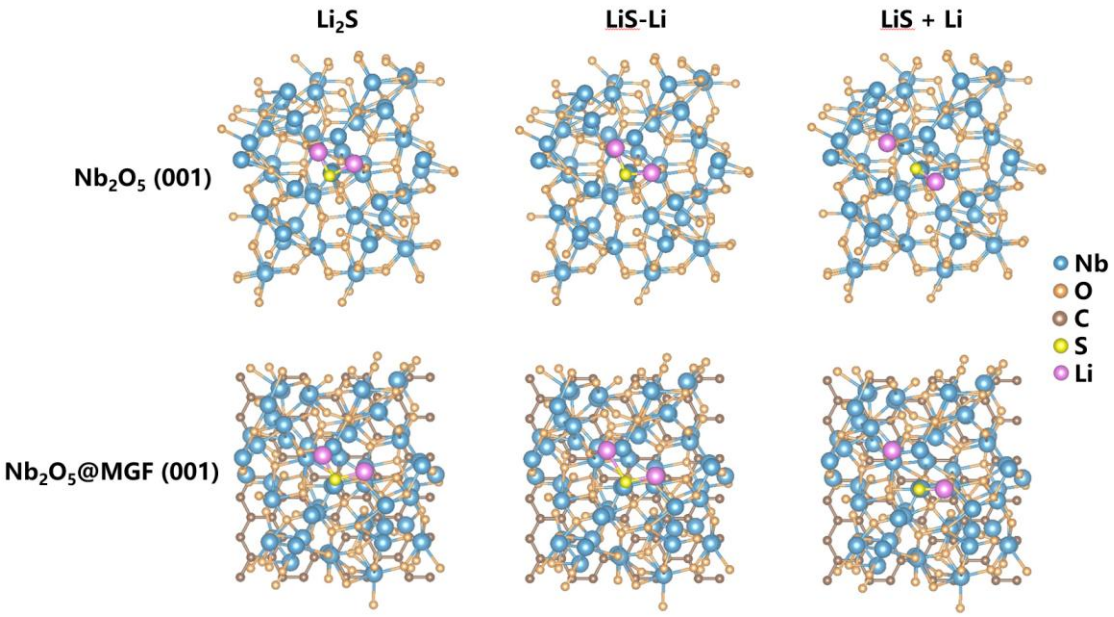

Figure S18. Li_2S decomposition path on Nb_2O_5 (001) facet and (b) Nb_2O_5@MGF (001) facet.

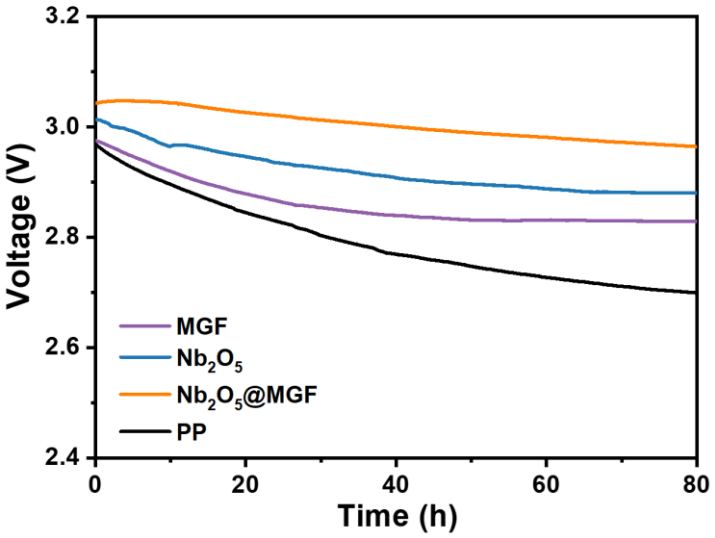

Figure S19. Open circuit voltage versus time curves.

The superior retention of the Nb_2O_5@MGF cell underscores its effectiveness in suppressing the shuttle effect.

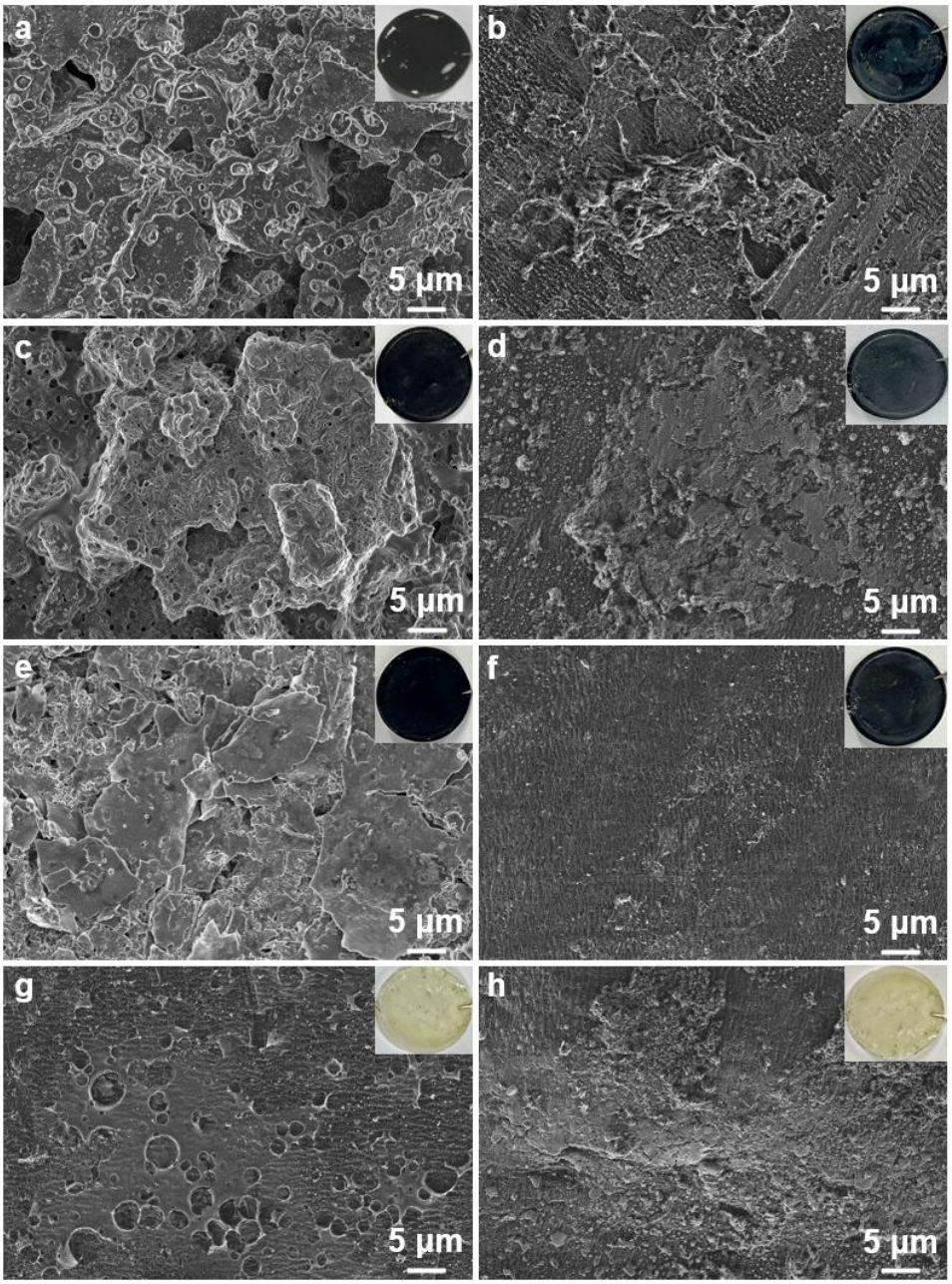

Figure S20. SEM images and photographs (inset) of the front side of separators after 100 cycles at 0.2 C: (a) MGF/PP, (c) Nb_2O_5/PP, (e) Nb_2O_5@MGF/PP, and (g) PP separators. SEM images and photographs (inset) of the back side of separators after 100 cycles at 0.2 C: (b) MGF/PP, (d) Nb_2O_5/PP, (f) Nb_2O_5@MGF/PP, and (h) PP separators.

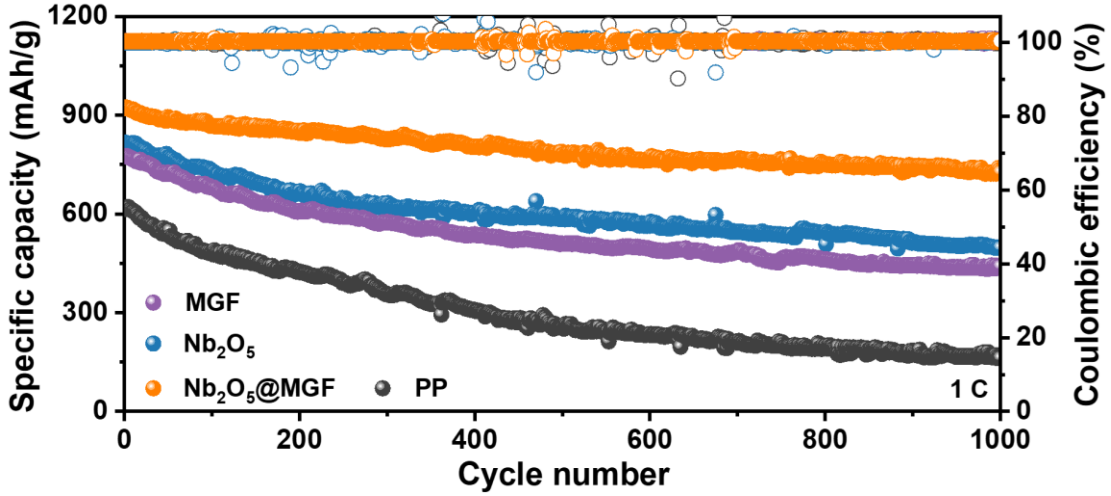

Figure S21. Cycling performance at 1 C for LSBs equipped with MGF/PP, Nb_2O_5/PP, Nb_2O_5@MGF/PP, and pristine PP.

Table S1. Performance comparison of the present Nb_2O_5@MGF/PP cell with recently reported LSBs using various interlayers.

Materials	S loading ($mg\ cm^{-2}$)	Current rate/Number of cycles	Initial Discharge Capacity ($mAh\ g^{-1}$)	Capacity retention (%)	Capacity decay rate (% per cycle)	References
Ru@Nb_2O_5@NC	0.9	1 C/500	1095	45%	0.11	[7]
	2	0.5 C/300	905	53%	0.16	
Nb_2O_5-3DG	-	0.5 C/200	1080	60%	0.20	[8]
NbB_2/rGO	3	0.1 C/80	516	83%	0.20	[9]
O-$Ti_{2.7}Nb_{0.3}C_2T_x$	0.4-0.5	0.2 C/100	865	58%	0.42	[10]
PA5-COOH/Nb_2C	1	1 C/500	799	72%	0.05	[11]
NbB_2@CC	1.2	0.2 C/100	1125	80%	0.20	[12]
	2.3	1 C/300	1050	72%	0.09	
Nb_2O_5@MGF	1.5	0.2 C/100	1275	85%	0.15	This work
		1 C/1000	922	79%	0.02	
	5	0.2 C/100	974	90%	0.10	

References

1. Y. Gao, Y. Deng, S. Xia, X. Xi, Z. Zhang, Y. Wang, D. Yang, T. Li and A. Dong, *Small*, 2024, **20**, 2402412.
2. G. Kresse and J. Furthmüller, *Comput. Mater. Sci.*, 1996, **6**, 15-50.
3. G. Kresse and J.Furthmüller, *Phys. Rev. B*, 1996, **54**, 11169-11186.
4. J. P. Perdew, K. Burke and M. Ernzerhof, *Phys. Rev. Lett.*, 1996, **77**, 3865-3868.
5. G. Kresse and D. Joubert, *Phys. Rev. B*, 1999, **59**, 1758-1775.
6. P. E. Blöchl, *Phys. Rev. B*, 1994, **50**, 17953-17979.
7. P. Yang, C. Lin, J. Zhou, L. Meng, Y. Zhang and H. Fan. *Chin. Chem. Lett.*, 2025, 111810.
8. R. Chu, T. Nguyen, H. Song, Y. Bai, D. Tran, N. Kim and J. Lee. *Appl. Catal. B Environ.*, 2024, **352**, 124030.
9.Y. Li, Z. Wang, H. Gu, H. Jia, Z. Long and X. Yan. *ACS Nano*, 2024, **18**, 8863-8875.
10. Q. Wang, B. Deng, X. Zhang, L. Cao, K. Wang, W. Yao, C. Chen, H. Zhao and J. Xu. *J. Materiomics*, 2025, **11**, 100920.
11. X. Liu, D. He, X. Liu, C. Fu, W. Gu, J. Lu, C. Wang, T. Wang. *Appl. Surf. Sci.*, 2025, **685**, 161985.
12. L. He, Y. Cheng, Q. Li, H. Zhao, M. Wang, X. Shi, X. Zou, Y. Wang, Y. Wei. Chem. Eng. J., 2023, **453**, 139566.